urban science

MDPI

Article

Long-Term Urban Thermal Dynamics and Land Use Transformation in Košice, Slovakia: A Landsat Time Series Analysis (1985–2025)

Zofia Kuzevicova [1,*], Stefan Kuzevic [2] and Diana Bobikova [1]

[1] Institute of Geodesy, Cartography and Geographical Information Systems, Faculty of Mining, Ecology, Process Control and Geotechnology, Technical University of Kosice, Letna 9, 042 00 Kosice, Slovakia; diana.bobikova@tuke.sk
[2] Institute of Earth Resources, Faculty of Mining, Ecology, Process Control and Geotechnology, Technical University of Kosice, Letna 9, 042 00 Kosice, Slovakia; stefan.kuzevic@tuke.sk
* Correspondence: zofia.kuzevicova@tuke.sk

Abstract

This paper focuses on the analysis of long-term land surface temperature (LST) dynamics and land-use changes in the city of Košice, Slovakia, during the period 1985–2025. The analysis is based on multi-temporal Landsat satellite imagery processed within a geographic information system (GIS) environment. Non-parametric statistical methods, including the Mann–Kendall trend test and the Theil–Sen slope estimator, were applied at the pixel level to identify the direction, magnitude, and statistical significance of long-term trends. Land-use changes were evaluated using CORINE Land Cover data together with the NDVI and NDBI spectral indices. The results revealed a statistically significant increase in land surface temperature across almost the entire urban area, with the mean LST increasing by 5.83 °C between 1985 and 2025. The analysis also confirmed a strong positive correlation between built-up areas and LST values, whereas vegetation cover exhibited a significant cooling effect represented by a strong negative correlation with surface temperature. Spatial analysis identified pronounced warming hotspots concentrated mainly in industrial and newly urbanized areas, while vegetation-stabilized zones showed lower warming intensity or localized cooling trends. The findings highlight the dominant influence of urbanization processes on the city's thermal regime and emphasize the importance of urban vegetation as a key adaptation element for mitigating the surface urban heat island effect. The study also illustrates the added value of integrating remote sensing data, GIS tools, and pixel-based trend analysis in the assessment of long-term changes in the urban thermal environment of medium-sized Central European cities. The results provide a spatial basis for climate adaptation planning and future assessments of urban thermal comfort and environmental quality.

Keywords: land surface temperature; Landsat; NDVI; NDBI; urbanization; thermal hotspots

Check for updates

Academic Editors: Veronica Martins Gnecco, Luka Pajek and Marco Arnesano

Received: 14 May 2026
Revised: 24 June 2026
Accepted: 24 June 2026
Published: 26 June 2026

Copyright: © 2026 by the authors. Licensee MDPI, Basel, Switzerland. This article is an open access article distributed under the terms and conditions of the Creative Commons Attribution (CC BY) license.

1. Introduction

Rapid and long-term urbanization may induce several negative environmental impacts. Built-up surfaces absorb and subsequently re-radiate larger amounts of solar radiation [1,2], which may lead to increased surface temperatures and alterations in the thermal regime of urbanized environments compared with surrounding rural areas. In the literature, this phenomenon is referred to as the urban heat island (UHI) effect [3,4]. The UHI can affect

human physical health [5,6], mental health [7], temperature-related mortality [8–10], and urban economic productivity [11]. Due to the increasing intensity of urbanization and climate change, the urban thermal environment and long-term thermal dynamics of cities have become important research topics in urban climatology, ecology, and urban planning.

The formation of the urban thermal environment and the emergence of the UHI effect are influenced by several factors [12], including terrain morphology, climatic conditions, urban structure, material properties [13], and vegetation cover [14,15]. In different types of urban environments, these factors may affect the spatial distribution of surface temperature and the intensity of heat accumulation in different ways, highlighting the need to analyze their interactions and sensitivities [16]. Such assessments make it possible to identify key parameters that are crucial for urban planning, design, and strategic decision-making.

Land surface temperature (LST) represents one of the key parameters used in the analysis of the spatial and temporal dynamics of the urban thermal environment. Remote sensing data [17,18] enable the assessment of spatial patterns of urban thermal dynamics, the identification of thermal hotspots, and the analysis of heat accumulation areas associated with land-use change and urbanization. Studies focused on UHI analysis [19–21] have successfully used remote sensing data to investigate the spatio-temporal dynamics of land surface temperature and evaluate the effects of urban expansion and land-use change on urban thermal environments. Ref. [22] emphasizes that remote sensing provides a comprehensive synoptic view of urbanized areas, enabling the identification of specific thermal response patterns of different surface types, including locations with intensive heat accumulation that are difficult to capture using stationary measurements due to their limited spatial coverage.

In the spatial analysis of pixel-level LST time series, it is necessary to determine not only the direction of temperature change (increasing, decreasing, or stable), but also its intensity and statistical significance. The non-parametric Mann–Kendall test [23,24] is commonly used to detect the significance of trends, while the Theil–Sen slope estimator [25,26] is applied to quantify trend magnitude. Over the past two decades, these non-parametric statistical methods have become standard tools for detecting and quantifying monotonic trends in environmental, hydrometeorological, and climatic time series [27,28]. These approaches are particularly important in the analysis of long-term LST development and urban thermal dynamics because of their robustness against outliers and seasonal variability in the data [29,30].

In Slovak cities, research on the urban thermal environment is primarily focused on the analysis of LST, thermal dynamics, and the surface urban heat island (SUHI) effect. Holec et al. [31] contributed to the understanding of long-term urban thermal development by analyzing changes in the heat island effect in Bratislava and Trnava during the period 1998–2016. Their study demonstrated a direct relationship between the expansion of impervious surfaces and increasing SUHI intensity. The MUKLIMO model [32] has been successfully applied in this region for modeling microclimatic conditions and predicting thermal stress. A study conducted in the city of Prešov [33] employed machine learning algorithms (random forest) for thermal data downscaling to a spatial resolution of 10 m, enabling a more detailed identification of local thermal patterns than is possible using the original Landsat resolution.

In [34], the authors analyzed the spatial distribution of LST within the city of Košice and its relationship with land use, highlighting the important role of urban vegetation in mitigating the urban heat island effect. Subsequent research in this field focused on advanced approaches to urban thermal environment modeling, including physically based LST modeling using 3D urban structure models capable of accounting for shading effects and surface orientation [35]. In [36], they combined the local climate zones concept, satellite

data (Landsat, ECOSTRESS), microclimatic modeling (ENVI-met), and in situ measurements. The results confirmed that integrating remote sensing data with microclimatic modeling is essential for understanding the daily overheating cycle of urban structures. Ref. [37] quantified the daily dynamics of thermal stress in the center of Košice during a heat wave using the ENVI-met model and high-resolution data (Sentinel-2, LiDAR), identifying critical heat accumulation areas and urban thermal hotspots, while Ref. [38] analyzed the structure of urban vegetation in Košice using 3D spatial data.

The aim of this study was to analyze the long-term development of LST and the spatial dynamics of the urban thermal environment in the city of Košice during the period 1985–2025, and to assess the influence of land-use change on the thermal regime of the urbanized landscape. In this context, the study addresses research questions related to the existence and spatial variability of LST trends, the spatial dynamics of the urban thermal environment, and the relationships between LST and land-use indicators like the normalized difference vegetation index (NDVI) and the normalized difference built–up index (NDBI). Based on these questions, hypotheses were formulated assuming an increasing LST trend, a positive relationship between built-up areas and surface temperature, and a negative effect of vegetation on LST values.

The novelty of this study lies in the application of a pixel-based trend analysis of a 40-year Landsat satellite time series (1985–2025) using non-parametric statistical methods (Mann–Kendall test and Theil–Sen slope estimator), enabling the quantification of the direction, intensity, and statistical significance of long-term LST trends in the urban environment. Unlike many previous studies focused on shorter time periods or isolated indicators, this paper integrates LST, NDVI, NDBI, and land-use change data, providing a comprehensive assessment of the relationship between urbanization processes and the thermal regime of the city. The significance of the study also lies in the analysis of urban thermal dynamics and land-use transformation over a 40-year period (1985–2025) using a consistent Landsat time series. Furthermore, the results enable the identification of long-term thermal hotspots and areas with significant vegetation cooling effects, providing a basis for climate-adaptive urban planning.

2. Materials and Methods

2.1. Study Area

In this study, the city of Košice was selected as the study area. Košice is the second largest city in Slovakia and has undergone dynamic urban development both historically and in recent decades. The city has experienced intensive growth in sectors such as construction, energy, and transportation, which may significantly contribute to changes in urban thermal conditions. The gradual reduction in green spaces and natural areas, particularly due to construction activities, increases the city's vulnerability to climate change impacts. For this reason, the analysis of urban thermal dynamics is of considerable importance.

The city of Košice is in eastern Slovakia (Figure 1) within the Košice Region, in the Košice Basin along the Hornád River valley. Administratively, the city is divided into 22 city wards with its own local self-government and four administrative districts. The total area of the city is 24,373.4 ha, with a population of 223,678 inhabitants as of 31 December 2024. Elevation ranges from 177 to 819 m above sea level.

Košice is characterized by a heterogeneous and polycentric urban structure shaped by historical development, socialist industrialization, and post-socialist transformation [39]. The city core consists of a compact radial-concentric medieval structure with adjacent 19th-century block development. A dominant component of the residential environment is represented by large housing estates built between the 1960s and 1980s, characterized by open urban composition and integrated green infrastructure (as shown in Figure 1c).

Industrial zones are concentrated in the southern part of the city, while peripheral areas have undergone substantial residential expansion. These complex transformations of the metropolis [40] have resulted in pronounced spatial differentiation of the urban environment, where compact historical structures, housing estates, and newly developed commercial zones coexist. The current spatial organization and functional land use are defined by the urban plan of the city of Košice [41].

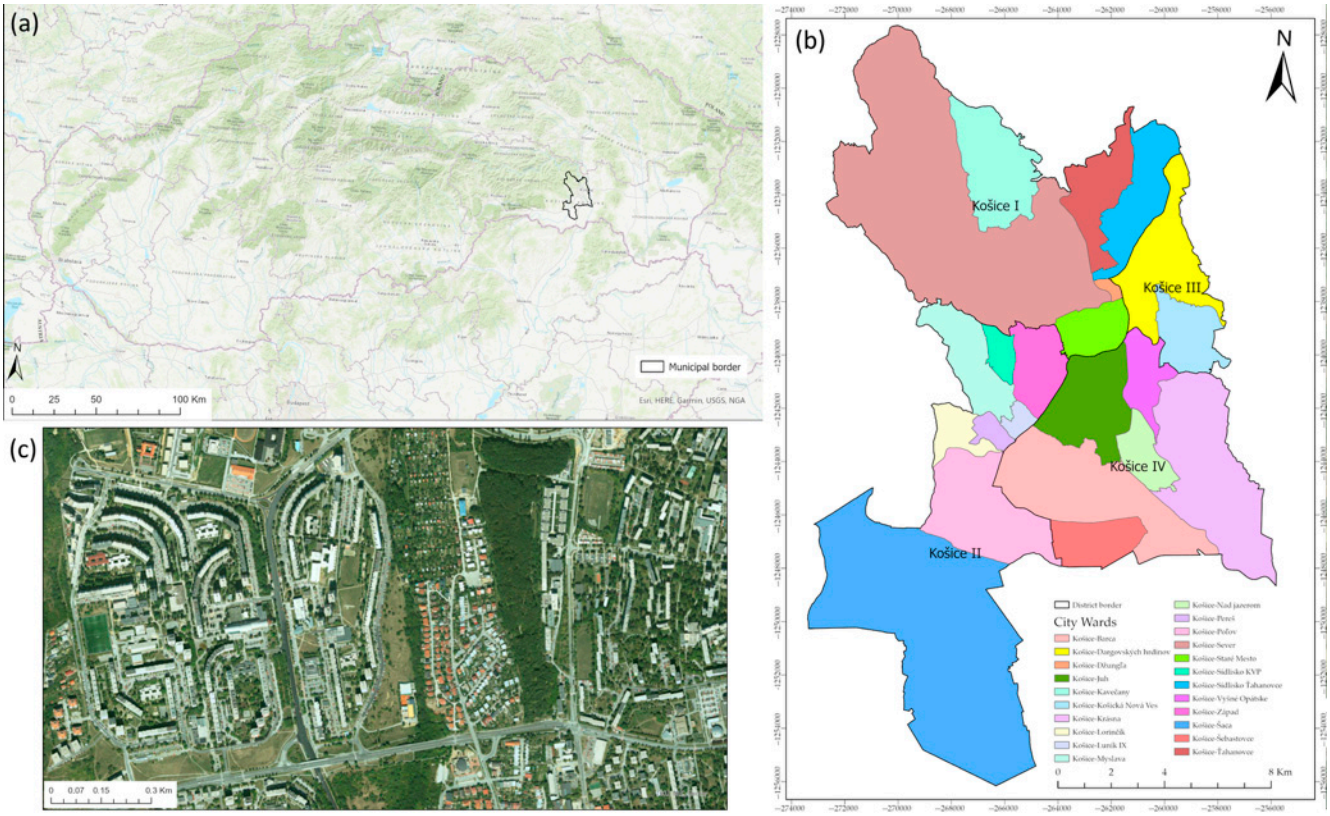


Figure 1. Study area—city of Košice: (**a**) location of Košice within Slovakia; (**b**) administrative districts and city wards of the city of Košice; (**c**) detailed view of the urban structure in Košice—KVP housing estate.

According to the Konček climate classification [42], the study area belongs to a warm, moderately dry climatic region with cold winters. The mean annual air temperature is approximately 8.6 °C, while the average annual precipitation ranges from 550 to 800 mm. According to Meteoblue (www.meteoblue.com) climate normals, the average daily maximum air temperatures during the summer months (June–August) typically range between 25 and 27 °C, whereas the average daily minimum temperatures are approximately 14–15 °C.

2.2. Methodology

In this study, the research workflow consisted of study area selection, data collection, preparation, and preprocessing, followed by analytical procedures including the calculation of LST, NDVI, and NDBI indices.

I. Data Collection

The datasets used in this study were obtained from freely available sources. Detailed characteristics of each dataset are provided in the following sections. All data were processed and analyzed in ArcGIS Pro 3.5.0 using the Slovak national coordinate reference system S–JTSK/Krovak East North (EPSG:5513).

II. Data Preparation and Preprocessing

During preparation, all input datasets were clipped to the boundaries of the study area using the Clip tool in ArcGIS Pro. Landsat datasets were processed using the USGS Landsat QA Toolbox.

III. Index Calculation and Data Analysis

Different statistical aggregation approaches were applied for July and August data depending on the characteristics of the analyzed variables. For LST, the arithmetic mean was used to represent the overall thermal state of the study area and to capture the average intensity of thermal conditions during the analyzed period. In contrast, the median was applied for NDVI values because it is less sensitive to extreme observations that may result from residual cloud contamination, atmospheric noise, or seasonal vegetation variability, thereby providing a more robust estimate of vegetation conditions. For NDBI, the arithmetic mean was used because this index more consistently represents the proportion of built-up and impervious surfaces, while its spectral variability within the time series is generally lower compared with vegetation indices. The application of these statistical approaches improved the robustness of the results and reduced the influence of anomalous values within the time series.

Subsequently, non-parametric trend analyses were applied to the NDVI and LST time series using the Mann–Kendall test and Sen's slope estimator in order to identify the direction, magnitude, and statistical significance of long-term changes in the analyzed parameters.

2.2.1. Landsat Imagery

This study used Landsat satellite imagery obtained from the USGS Earth Explorer portal (USGS EarthExplorer, https://earthexplorer.usgs.gov, accessed on 12 December 2025) in GeoTIFF format. Data acquisition focused on the summer season, specifically July and August, while one of the primary selection criteria was minimal cloud cover. All available Landsat observations from missions 4, 5, 7, 8, and 9 acquired between 1985 and 2025 were included in the analysis. The year 2012 was excluded because imagery of sufficient quality was not available. All raster datasets were processed at a spatial resolution of 30 m, which is suitable for assessing long-term urban thermal dynamics and land-use changes at the city scale, although smaller urban features may not be fully represented.

The quality of the input data was ensured through a combination of cloud masking and the removal of low-quality observations based on the QA_PIXEL band. Clouds, cloud shadows, and invalid pixels were removed using the USGS Landsat QA Toolbox. In the case of Landsat 8 and Landsat 9 imagery, cirrus clouds were also excluded from the analysis because they may affect the accuracy of LST estimation.

LST was derived from Landsat Collection 2 Level-2 products, specifically from bands ST_B6 (Landsat 4, 5, and 7) and ST_B10 (Landsat 8 and 9), which provide atmospherically corrected surface temperature products. LST values in Kelvin were converted to degrees Celsius. The derived LST values represent surface temperatures recorded during satellite overflights under clear-sky conditions and should not be interpreted as the air temperature at the Earth's surface.

2.2.2. CORINE Land Cover

CORINE Land Cover data obtained from the Copernicus Land Monitoring Service Portal [43] were used to create the land-use layer. The CORINE Land Cover database has a minimum mapping unit of 25 ha for areal features and a minimum width of 100 m for linear features. For the purposes of this study, datasets from 1990 and 2018 were used, representing the initial and recent periods of the analyzed surface temperature time series.

The year 1990 was selected as the closest available reference year to the beginning of the analyzed period (1985), while 2018 represents the most recent fully available dataset for Slovakia. CORINE Land Cover classes were reclassified into the following categories: artificial surfaces, agricultural areas, forest and semi-natural areas, and water bodies.

2.2.3. Trend Analysis Methods

The statistical significance of trends in the LST time series during the period 1985–2025 was analyzed using the Mann–Kendall test. Trend magnitude was quantified using Sen's slope estimator. Both methods belong to non-parametric statistical approaches and are characterized by robustness against missing values and outliers [44,45].

The Mann–Kendall test evaluates monotonic trends in a time series by comparing each observation with all subsequent values in the series. For each pair of observations (x_j,x_k), where j > k, the direction of the difference between the values (positive or negative) is determined. The test is non-parametric and is based on the signs of differences between observation pairs rather than on their absolute values. The sum of these directional signs forms the Mann–Kendall test statistic S [46] (Equation (1)).

$$S = \sum_{k=1}^{n-1} \sum_{j=k+1}^{n} sgn(x_j - x_k), \quad (1)$$

where n is the length of the time series, x_j and x_k are values in the time series at observations k and j (j > k), and sgn($x_j - x_k$) is the sign function calculated using Equation (2).

$$sgn(x_j - x_k) = \begin{cases} +1; if\ x_j - x_k > 0 \\ 0; if\ x_j - x_k = 0 \\ -1; if\ x_j - x_k < 0 \end{cases}, \quad (2)$$

For n ≥ 10, the Mann–Kendall test statistic S approaches a normal distribution with variance Var(S) calculated according to Equation (3).

$$Var(S) = \frac{n(n-1)(2n+5) - \sum_{p=1}^{q} tp(tp-1)(2tp+5)}{18}, \quad (3)$$

where n is the length of the time series, q is the number of tied groups, and t_p is the number of equal observations within the time series.

The normalized test statistic Z was calculated according to Equation (4).

$$Z = \begin{cases} \frac{S-1}{\sqrt{Var(S)}}, if\ S > 0 \\ 0, ak\ S = 0 \\ \frac{S+1}{\sqrt{Var(S)}}, if\ S < 0 \end{cases}, \quad (4)$$

The calculated Z value was used to assess the statistical significance of trends in the time series. The significance level α was applied to test both increasing and decreasing trends. At a significance level of α = 0.05, the trend was considered statistically significant when Z > ±1.96. A positive Z value indicates an increasing trend, whereas a negative Z value indicates a decreasing trend. A value close to zero corresponds to the absence of a statistically significant trend.

Trend magnitude was determined using Sen's slope estimator (Equation (5)).

$$Q_i = \frac{x_j - x_k}{j - k} \text{ for } i = 1, \ldots, N, \quad (5)$$

where Q_i represents the slope between two observations corresponding to years j and k (j > k), and N = n(n − 1)/2 is the total number of possible slope pairs. Sen's slope estimator is defined as the median of all Q_i values.

2.2.4. The Normalized Difference Vegetation Index (NDVI)

NDVI is a simple method used for vegetation quantification by evaluating the difference between near-infrared radiation, which is strongly reflected by vegetation, and red radiation, which is absorbed by vegetation. NDVI enables the assessment of vegetation growth conditions and is therefore widely used in studies of land-cover dynamics and urban thermal environment dynamics including UHI [47,48].

NDVI was calculated using the commonly applied equation (Equation (6)) [17].

$$NDVI = \frac{(NIR - Red)}{(NIR + Red)}, \quad (6)$$

where NIR represents the near-infrared band (Band 4 for Landsat 4–7 and Band 5 for Landsat 8–9), and Red represents the red band (Band 3 for Landsat 4–7 and Band 4 for Landsat 8–9).

The resulting raster layers contain values ranging from –1 to 1, where higher positive values (close to +1) correspond to dense vegetation, while values close to zero or negative values (approaching -1) indicate water bodies and non-vegetated surfaces. The calculated raster datasets were subsequently used for the analysis of vegetation-cover changes within the study area.

2.2.5. The Normalized Difference Built–up Index (NDBI)

The NDBI is one of the most commonly used spectral indices for identifying built-up areas and enables the effective separation of impervious surfaces from other land cover components [49]. It is calculated as the difference between the spectral reflectance values of the shortwave infrared (SWIR) and near-infrared (NIR) bands, divided by their sum (Equation (7)) [50].

$$NDBI = \frac{(SWIR - NIR)}{(SWIR + NIR)}, \quad (7)$$

where NIR refers to the near-infrared band (Band 4 for Landsat 4–7 and Band 5 for Landsat 8–9), and SWIR refers to the shortwave infrared band (Band 5 for Landsat 4–7 and Band 6 for Landsat 8–9).

The NDBI values range from -1 to +1, with positive values being typical of built-up areas. Low positive values (close to 0) correspond to transitional or mixed zones and bare soil. Negative values close to -1 are generally associated with non-built-up areas, such as vegetation or water bodies.

3. Results

The calculated average values of LST and NDBI and the median values of the NDVI index for individual years are presented in Appendix A, Table A1. For clarity, the main text presents spatial analyses for the baseline year (1985) and the target year (2025), along with the results of trend analyses.

3.1. Land Use Analysis

For the initial assessment of land use change and the characterization of landscape structure, CORINE Land Cover (CLC) data covering the period 1990–2018 were utilized. A comparison between the selected years (Table 1) revealed significant changes in the spatial organization of land use within the administrative boundaries of the city of Košice.

The results indicate an increase in artificial surfaces, which expanded by 209.90 ha. This increase is likely associated with urbanization processes and the expansion of built-up areas, particularly in the peripheral parts of the city. In contrast, the area of agricultural areas decreased by 751.55 ha over the studied period, indicating a gradual transformation of

agricultural land into built-up or other land use types. At the same time, an increase in forest and semi-natural areas was observed, with an expansion of approximately 538.46 ha. This increase may be related to natural vegetation succession or changes in land management practices. The area of water bodies remained relatively stable over the study period, with only a slight increase of 3.19 ha.

Table 1. CORINE Land Cover (CLC) Level 1 classes for 1990 and 2018.

CLC Code Level 1	1990 [ha]	1990 [%]	2018 [ha]	2018 [%]	2018–1990 [ha]
1 Artificial surfaces	6509.88	26.70	6719.78	27.57	209.90
2 Agricultural areas	10,021.59	41.11	9270.04	38.03	–751.55
3 Forest and semi natural areas	7818.18	32.07	8356.64	34.28	538.46
5 Water bodies	27.56	0.11	30.75	0.13	3.19

A typical example of land use transformation is the area of the former Bankov quarry. The onset of surface magnesite mining dates back to 1901. Mining activities were terminated between 1996 and 1999, and the processing plant was subsequently closed. In the CORINE Land Cover dataset from 1990, the area was classified as 132 dump sites (32.2 ha) and 131 mineral extraction sites (Figure 2a). Following the cessation of mining activities, the area underwent a gradual natural transformation. By 2000, spontaneous vegetation succession was observed, and the site was classified as broad-leaved forest (33.3 ha) (Figure 2b). By 2018, further ecological development had occurred, and the area was classified as mixed forest (33.3 ha) (Figure 2c).

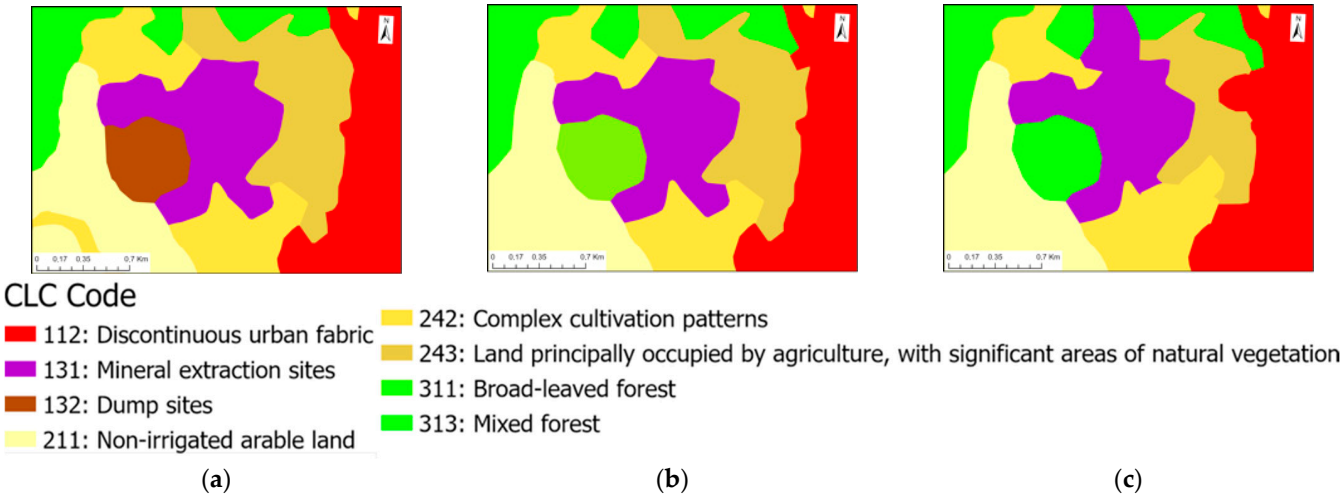


Figure 2. CLC classes in the selected Bankov area: (**a**) 1990; (**b**) 2000; (**c**) 2018.

The study area was further analyzed using the normalized difference built-up index (NDBI), which enables the identification of built-up and urbanized areas based on the spectral characteristics of Landsat satellite imagery. For comparison, the boundary years 1985 and 2025 were selected. The resulting NDBI layers are presented in Figure 3. The NDBI values were classified into five categories, ranging from very high to very low, similar to the approach adopted by Cetin et al. [48].

The results of the NDBI analysis for individual city wards are summarized in Appendix A, Table A2, while the classification intervals corresponding to the very low, low, moderate, high, and very high categories are provided in the legends of the respective NDBI maps. The table includes data for a total of 19 city wards of the city of Košice. However,

when comparing the years 1985 and 2025, not all wards could be included in the analysis. Specifically, in the wards of Košice-Sever, Košice-Nad jazerom, and Košice-Sídlisko KVP, areas with no data values were present in the 1985 dataset. For this reason, a direct comparison with the year 2025 was not possible for these areas.

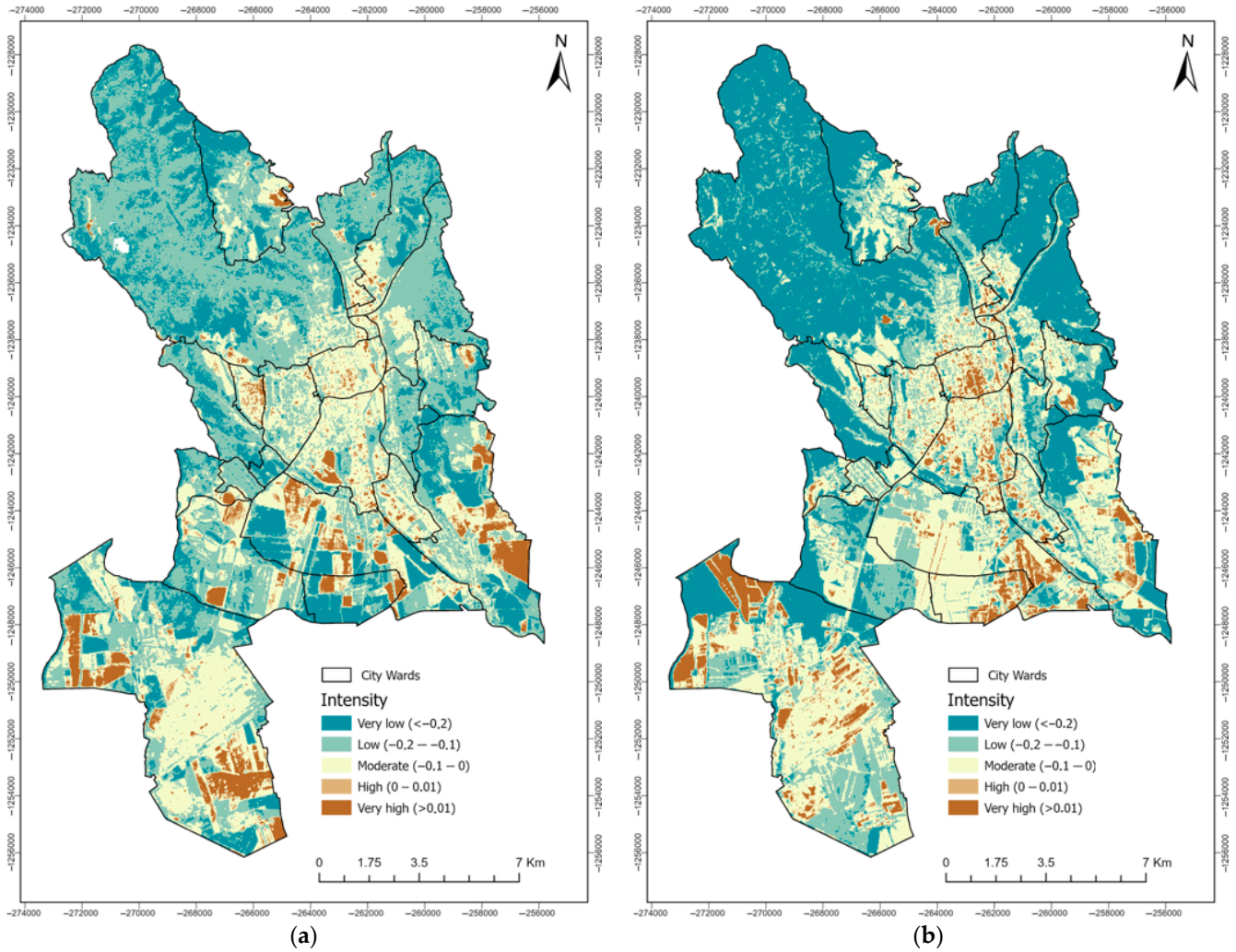


Figure 3. NDBI maps for the selected years: (**a**) 1985; (**b**) 2025.

The most significant changes were observed in several peripheral city wards. For instance, in the Košice-Šebastovce ward, the proportion of very low NDBI values decreased from 46.0% to 1.5%, while medium values increased from 12.3% to 64.0% and very high values increased from 12.5% to 17.0%. A similar trend was recorded in Košice-Barca, where the proportion of medium values increased from 33.0% to 54.7%, and in Košice-Krásna, where medium values increased from 22.7% to 38.4%, while very high values decreased from 13.0% to 5.0%.

In the central part of the city, specifically in Košice-Staré Mesto, a marked increase in very high NDBI values was observed, rising from 5.4% in 1985 to 18.8% in 2025, indicating an intensification of urbanization and densification of the built-up structure. Similarly, in the Košice-Juh ward, the proportion of very high values increased from 8.0% to 12.1%.

In contrast, city wards with a higher proportion of vegetation maintained predominantly low NDBI values. For example, in Košice-Kavečany, low and very low values accounted for up to 72.3% in 2025 (a decrease from 78.3% in 1985), while the proportion of high and very high values remained negligible (0.3%). A similar pattern was observed in Košice-Myslava, where low and very low values reached 81.5% in 2025.

3.2. NDVI

To eliminate extreme values and reduce the influence of residual cloud contamination, the median NDVI for the July–August period was calculated for each year. Figure 4 illustrates the distribution of NDVI classes for 1985 (Figure 4a) and 2025 (Figure 4b). The NDVI values were classified into five categories reflecting varying vegetation cover density. Lower values represent built-up areas and bare soil, whereas higher values correspond to progressively denser vegetation.

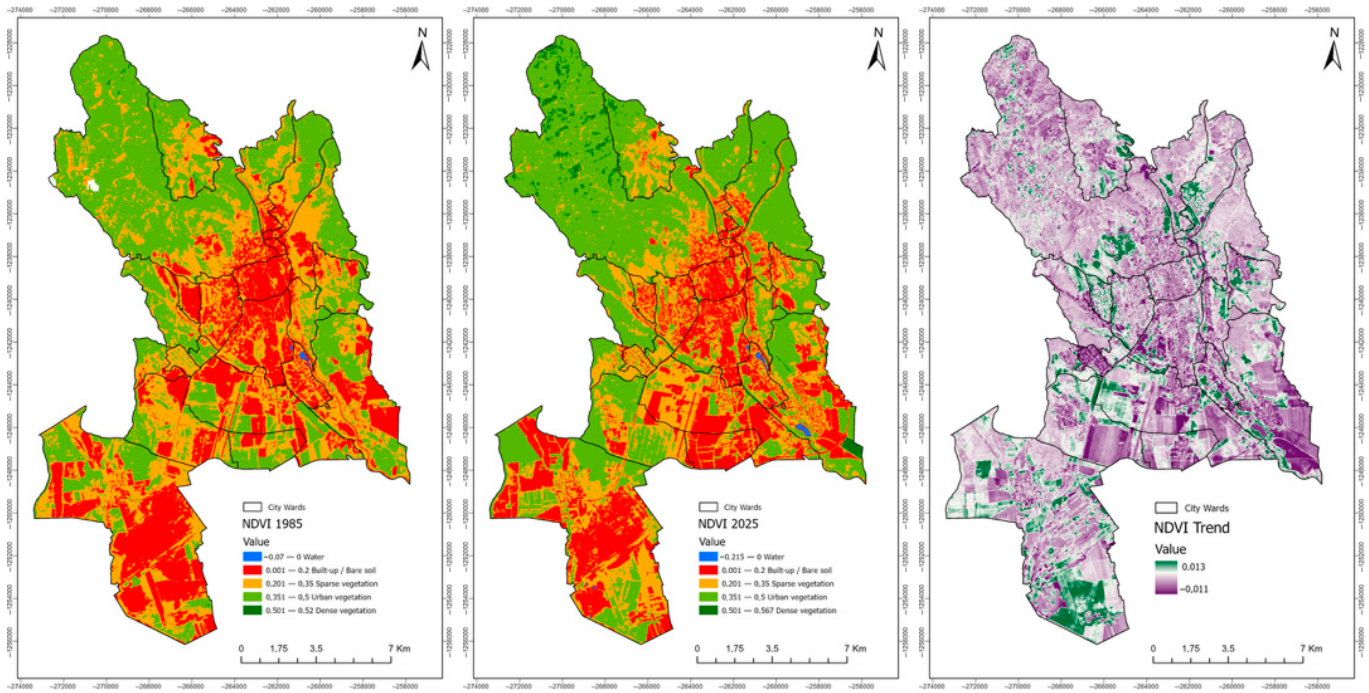


Figure 4. NDVI in the study area: (**a**) NDVI values in 1985; (**b**) NDVI values in 2025; (**c**) Sen's slope NDVI trend in 1985–2025.

A comparison of 1985 and 2025 highlights changes in vegetation cover within the study area. In 2025, areas with NDVI values exceeding 0.05 were already present, indicating denser vegetation cover. In 1985, NDVI values ranged from −0.07 to 0.52, whereas in 2025, the minimum value was −0.22 and the maximum value reached 0.57.

The Sen's slope values for the NDVI time series (Figure 4c) ranged from −0.011 to 0.013. Positive values, identified across approximately 77% of the study area, indicate an increasing trend and a potential rise in vegetation cover. In contrast, negative values, covering approximately 23% of the area, indicate a decreasing NDVI trend associated with vegetation loss or degradation.

3.3. The LST Results

LST maps are presented in Figure 5. In 1985, LST values ranged from 15.7 °C to 51.2 °C (Figure 5a), whereas in 2025 they ranged from 23.3 °C to 59.3 °C (Figure 5b). Figure 5c presents the Sen's slope values for the LST time series, illustrating the spatial trend of temperature changes over the study period.

The results of the Sen's slope analysis for the LST time series indicate an overall increasing trend in LST. Positive values were identified across approximately 99.99% of the study area, while negative values occurred only sporadically. This finding suggests a widespread increase in surface temperature throughout the entire area. Negative values, representing a decreasing LST trend, were observed only locally, particularly in the Bankov

area (Figure 2). This development is associated with the cessation of mining activities and subsequent natural reclamation of the site, which led to gradual vegetation recovery and a reduction in LST. The results of the statistical and correlation analyses are presented in Tables 2 and 3 below.

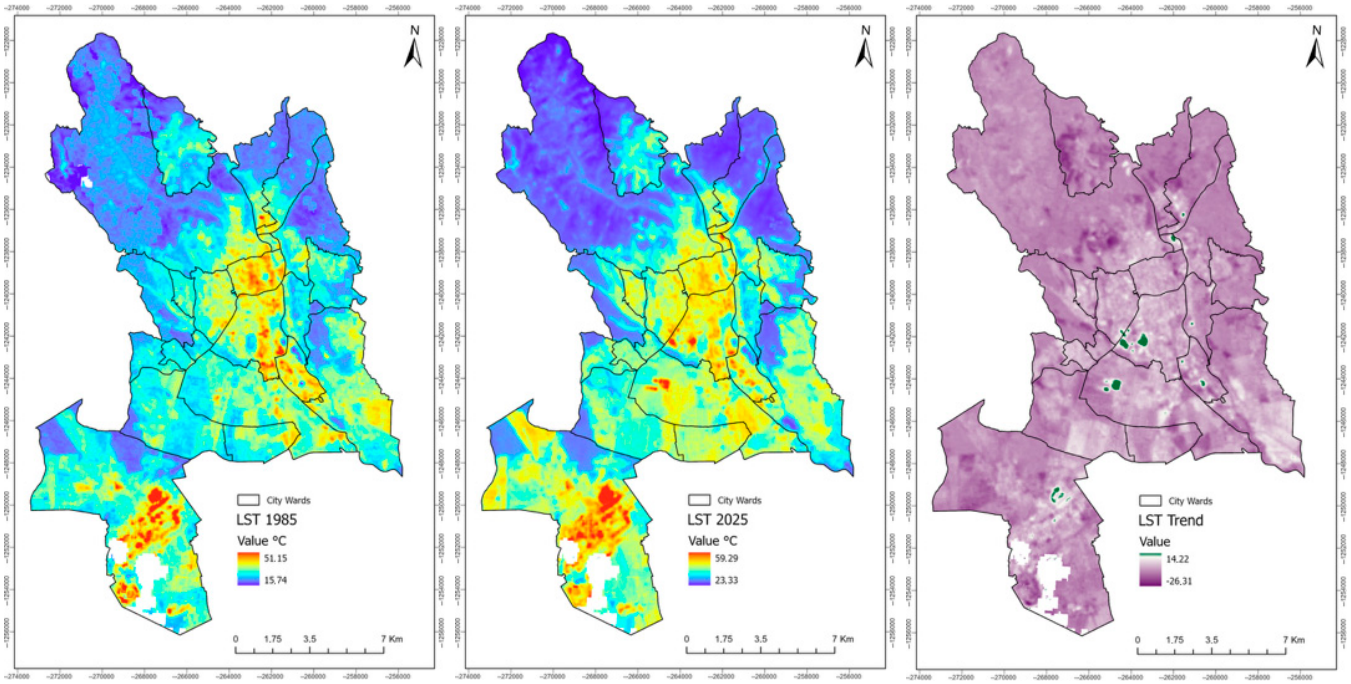


Figure 5. Mean July–August LST values in the study area: (**a**) mean LST in July–August 1985; (**b**) mean LST in July–August 2025; (**c**) Sen's slope LST trend in 1985–2025.

Table 2. Development of LST and indices (1985–2025).

Parameter	Mean		Rozdiel
	1985	2025	
LST	26.12	31.95	5.83
NDVI	0.29	0.32	0.03
NDBI	−0.13	−0.14	−0.01

Table 3. Correlation matrix.

Relationship	1985	2025
LST vs. NDVI	−0.72	−0.81
LST vs. NDBI	0.67	0.83

Descriptive statistical analysis revealed an increase in mean LST in the city of Košice by 5.83 °C, rising from 26.12 °C in 1985 to 31.95 °C in 2025. Over the studied period, an increase in maximum temperatures from 51 °C to 59 °C was also observed. The mean value of the vegetation index (NDVI) increased by 0.03, whereas the mean built-up index (NDBI) remained relatively stable, with a slight decrease of 0.01.

The correlation analysis confirmed a linear relationship between land use and LST. For the LST vs. NDVI relationship, the negative correlation strengthened from −0.72 to −0.81. A more pronounced change was observed for the LST vs. NDBI relationship, where the correlation coefficient increased from 0.67 to 0.83. The coefficient of determination (R^2) in 2025 indicates that NDVI explains 65.6% of the spatial variability in temperature (an

increase of 13.8% compared to 1985), while for NDBI, the explanatory power increased from 45% to nearly 69%.

4. Discussion

The results of the CORINE Land Cover (CLC) analysis indicate a gradual transformation of the landscape within the administrative area of the city of Košice, reflected in estimated land-use and land-cover changes between 1990 and 2018. The increase in artificial surfaces and the decline in agricultural areas suggest an ongoing process of landscape artificialization according to the CORINE Land Cover classification. The increase in artificial surfaces at the expense of agricultural land (by more than 209 ha) from 1990 to 2018 is consistent with trends observed in other Central and Eastern European cities, where land market liberalization and transformation processes after 1989 have led to the conversion of agricultural landscapes into urban structures [51,52]. This development also reflects the broader processes of urban expansion and suburbanization, characterized by the spatial growth of built-up areas despite demographic stagnation or decline [53]. Similar land cover changes in Central and Eastern European cities have been quantified using remote sensing data, particularly long-term Landsat datasets enabling accurate land-use/land-cover change detection [54]. When interpreting changes in land use derived from the CORINE Land Cover database, it is necessary to take into account the minimum mapping unit of 25 ha, thematic generalization, and potential classification uncertainties, which may result in local changes in land cover going unrecorded and may affect the estimation of the extent of individual land use classes.

At the same time, an increase in forest and semi-natural areas was observed, which may be interpreted as a consequence of natural succession following the decline in industrial activities [55,56]. This process was identified in the Bankov area, where the transformation from a mining site to a forest ecosystem led to landscape regeneration and a reduction in LST. Similar cooling effects associated with vegetation recovery and land reclamation have been reported in post-mining landscapes in Central Europe and elsewhere [57–59]. The role of forest regeneration in mitigating local temperature increases has also been widely documented [60].

The comparison between 1985 and 2025 highlights a coupled relationship between urbanization and the thermal regime of the landscape. The shift of NDBI values toward higher categories indicates a gradual increase in urbanized and impervious surfaces, which play a key role in heat accumulation processes.

The strong positive correlation between NDBI and LST ($r = 0.83$) is consistent with previous studies [32,61–64]. Although NDBI exhibited a very strong correlation with surface temperature in 2025, its interpretation for built-up area identification in heterogeneous urban environments may be limited [49]. Spectral similarity between anthropogenic surfaces (concrete, asphalt) and bare agricultural soil leads to ambiguous classification, representing a known limitation of the NDBI [65,66].

In the context of Košice, characterized by a mosaic landscape structure and a high proportion of vegetation, the spectral signal is strongly influenced by biomass, resulting in average NDBI values shifting into the negative range (-0.14). Despite these limitations, the observed increase in the direct relationship between LST and NDBI by 0.16 and the improved explanatory power of the index (from 45% to 69%) indicate that modern impervious surfaces exhibit stronger heat accumulation than in the past [50,61]. Overall, the NDBI results reveal a highly differentiated urban development pattern, with the most pronounced changes occurring in peripheral and development zones, while vegetation-dominated areas maintain stable low NDBI values. Due to the 30 m spatial resolution of Landsat imagery,

the results primarily reflect city-scale patterns and may not fully represent small urban features or localized land-cover changes.

The NDVI index proved to be a key indicator of vegetation density and vegetation cover. Its negative correlation with LST confirms the important role of urban green infrastructure in mitigating the surface urban heat island intensity [63,67,68]. The analysis demonstrates that the cooling effect of vegetation has intensified over time, as evidenced by the strengthening of the negative correlation from −0.72 (1985) to −0.81 (2025). The coefficient of determination further indicates that vegetation currently explains up to 65.6% of the spatial variability in temperature, representing an increase of 13.8% compared to 1985. This suggests that under increasing summer temperature extremes, urban vegetation becomes a critical element of climate adaptation strategies [69,70].

Spatial trend analysis of LST using Sen's slope (Figure 5c) revealed pronounced local warming hotspots within Košice. These are primarily concentrated in the southern industrial zone, the airport vicinity, and newly developed commercial areas (e.g., Košice-Juh and Košice-Barca). In these locations, the maximum LST in 2025 reached nearly 60 °C, representing an increase of more than 8 °C compared to the 1985 maxima. This spatial pattern is consistent with studies indicating that industrial areas, logistics centers, and large impervious surfaces are among the most significant sources of heat accumulation in urban environments [19,29,48]. The intensification of temperature extremes in development zones also reflects ongoing urban landscape transformation, characterized by the replacement of vegetated surfaces with materials of high thermal capacity and low albedo [13,50]. The results suggest that the observed changes represent the combined effect of regional climate warming and local changes in land use, with urbanized areas showing a more pronounced rate of warming compared to sites with stable vegetation cover.

In contrast, a significantly lower rate of temperature increase was observed in stable residential areas with a high proportion of mature vegetation (e.g., Košice-Sever), confirming the essential role of urban biocenters and linear vegetation elements in mitigating urban heat effects. This relationship has been repeatedly confirmed in recent studies, highlighting a robust inverse relationship between vegetation cover and LST in urban environments and emphasizing the dominant role of evapotranspiration and shading in cooling urban surfaces [71–73]. Although LST does not directly represent near-surface air temperature, it is widely recognized as an effective indicator of spatial thermal patterns, heat accumulation processes, and the thermal response of urban surfaces. Although thermal comfort indices were not directly assessed, the identified warming hotspots and the observed relationship between vegetation cover and surface temperature provide valuable information for climate adaptation planning and future studies of outdoor thermal comfort and pedestrian-level environmental quality. The results thus indicate an increasing spatial polarization of the city's thermal regime, where the contrast between highly urbanized areas and vegetation-stabilized zones becomes increasingly pronounced under ongoing climate change.

5. Conclusions

The presented study confirms the existence of a pronounced and statistically significant increase in LST in the city of Košice over the period 1985–2025. The results further indicate a strong association between spatial patterns of land use and land surface temperature. The land-use/land-cover analysis demonstrates that built-up and impervious surfaces represent the primary drivers of heat accumulation, while vegetation cover plays a key role in mitigating the urban heat island effect. The results indicate a stronger association between vegetation cover and land surface temperature in 2025 compared with 1985, as reflected by the strengthening negative correlation between NDVI and LST. Conversely, the

increasing positive relationship between NDBI and LST indicates an intensifying influence of urbanization on the city's thermal regime.

Spatial analysis identified local areas of intense warming, particularly in industrial and newly developed areas characterized by extensive impervious surfaces, whereas areas with greater vegetation cover exhibited lower rates of warming.

At the same time, natural landscape regeneration processes were confirmed to contribute to local reductions in LST.

From a practical perspective, the results highlight the need for the systematic integration of green infrastructure elements into urban planning, including the preservation of existing vegetated areas, promotion of tree planting, and implementation of nature-based solutions. The findings of this study may serve as a basis for the development of adaptation strategies in urban environments, optimization of spatial planning, and management of urbanization processes aimed at reducing thermal stress on the population. The presented methodology can support future human-centered urban climate studies by identifying areas potentially exposed to increased thermal stress and by providing a spatial basis for climate adaptation measures aimed at improving urban livability.

From a research perspective, future work should focus on the integration of higher spatial and temporal resolution datasets (e.g., Sentinel or LiDAR), the application of advanced urban microclimate modeling techniques, and the use of machine learning approaches for a more precise identification of factors influencing LST. Future research should investigate how uncertainties in land-use and land-cover datasets influence the interpretation of observed relationships between land-cover change and land surface temperature dynamics. A promising direction for further research is also the integration of remote sensing data with in situ measurements and socio-environmental datasets, which may contribute to a more comprehensive assessment of urban heat island impacts on quality of life and support more effective planning of climate-resilient urban environments.

Author Contributions: Z.K.: Conceptualization, methodology, software, validation, formal analysis, resources, data curation, writing—original draft preparation, writing—review and editing, visualization; S.K.: Conceptualization, methodology, validation, formal analysis, investigation, data curation, writing—original draft preparation, visualization; D.B.: Conceptualization, methodology, formal analysis, investigation, data curation, writing—original draft preparation, visualization. All authors have read and agreed to the published version of the manuscript.

Funding: This research was funded by the Educational Grant Agency of the Ministry of Education, Research, Development, and Youth of the Slovak Republic KEGA No. 034TUKE–4/2026 and 020TUKE–4/2024.

Institutional Review Board Statement: Not applicable.

Informed Consent Statement: Not applicable.

Data Availability Statement: Data are available on reasonable request.

Conflicts of Interest: The authors declare no conflicts of interest.

Abbreviations

The following abbreviations are used in this manuscript:

LST	Land Surface Temperature
UHI	Urban Heat Island
SUHI	Surface Urban Heat Island
NDVI	The Normalized Difference Vegetation Index
NDBI	The Normalized Difference Built-up Index
CLC	CORINE Land Cover

Appendix A

Table A1. Mean LST, median NDVI, and mean NDBI values for the study area during the period 1985–2025.

Year	Mean LST °C	Median NDVI	Mean NDBI
1985	26.12	0.320	−0.132
1986	26.92	0.254	−0.114
1987	28.86	0.262	−0.102
1988	32.33	0.283	−0.112
1989	25.63	0.326	−0.133
1990	25.59	0.296	−0.066
1991	32.58	0.309	−0.144
1992	28.27	0.293	−0.113
1993	30.27	0.259	−0.095
1994	28.37	0.235	−0.089
1995	27.73	0.318	−0.125
1996	27.26	0.303	−0.107
1997	26.37	0.297	−0.105
1998	28.75	0.307	−0.120
1999	23.86	0.303	−0.133
2000	29.04	0.318	−0.121
2001	31.83	0.311	−0.136
2002	27.83	0.308	−0.152
2003	29.17	0.246	−0.093
2004	28.34	0.295	−0.116
2005	27.96	0.318	−0.138
2006	33.48	0.299	−0.127
2007	33.83	0.295	−0.102
2008	25.57	0.343	−0.131
2009	29.19	0.326	−0.120
2010	32.67	0.346	−0.134
2011	31.52	0.300	−0.138
2013	34.19	0.319	−0.118
2014	30.65	0.342	−0.141
2015	36.69	0.306	−0.121
2016	30.63	0.353	−0.144
2017	32.48	0.343	−0.135
2018	35.23	0.339	−0.127
2019	29.99	0.344	−0.140
2020	28.58	0.342	−0.154
2021	33.71	0.330	−0.155
2022	37.79	0.250	−0.096
2023	35.17	0.353	−0.126
2024	35.88	0.301	−0.108
2025	31.95	0.349	−0.137

Table A2. Results of the NDBI analysis (1—Very low, 2—Low, 3—Moderate, 4—High, 5—Very high).

City Wards	1985 [%]					2025 [%]				
	1	2	3	4	5	1	2	3	4	5
Košice—Kavečany	28.5	49.8	19.0	0.4	2.3	45.4	26.9	27.3	0.2	0.1
Košice—Ťahanovce	14.5	70.3	13.3	0.9	1.0	61.4	26.2	10.8	0.6	1.0
Košice—Staré Mesto	0.2	18.0	72.4	4.0	5.4	2.0	17.4	56.1	5.8	18.8
Košice—Lorinčík	19.2	46.2	28.1	1.7	4.8	33.3	25.3	34.7	3.6	3.0
Košice—Pereš	3.0	85.6	10.4	0.9	0.1	1.9	48.6	48.3	0.9	0.3
Košice—Myslava	27.3	58.8	13.0	0.6	0.4	61.2	20.3	18.1	0.2	0.2
Košice—Západ	1.5	45.2	50.1	1.6	1.7	7.3	29.1	57.4	2.4	3.8
Košice—Dargovských hrdinov	11.3	73.0	14.8	0.4	0.5	66.4	18.0	14.4	0.6	0.7
Košice—Košická Nová Ves	19.5	57.7	19.7	1.6	1.6	33.5	28.5	32.9	2.2	2.9
Košice—Barca	25.9	26.9	33.0	5.5	8.7	5.8	27.5	54.7	4.1	7.9
Košice—Šebastovce	46.0	25.8	12.3	3.3	12.5	1.5	10.0	64.0	7.5	17.0

Table A2. *Cont.*

City Wards	1985 [%]					2025 [%]				
	1	2	3	4	5	1	2	3	4	5
Košice—Krásna	24.4	36.3	22.7	3.6	13.0	30.7	21.7	38.4	4.2	5.0
Košice—Juh	3.2	27.9	58.5	2.4	8.0	8.4	20.5	52.9	6.1	12.1
Košice—Šaca	14.5	30.2	41.6	3.3	10.4	16.4	27.1	41.0	4.2	11.3
Košice—Poľov	14.9	49.7	26.9	3.5	4.9	29.5	40.8	28.5	0.8	0.5
Košice—Sídlisko Ťahanovce	23.8	54.9	18.7	1.1	1.6	66.9	15.3	15.5	0.7	1.5
Košice—Džungľa	0.0	15.9	76.2	4.4	3.4	1.5	18.2	65.3	5.2	9.8
Košice—Vyšné Opátske	17.5	65.6	16.5	0.1	0.3	26.5	39.2	31.9	0.9	1.5
Košice—Luník IX	44.1	47.6	8.3	0.0	0.0	21.4	23.1	54.7	0.3	0.5

References

1. Hang, J.; Zeng, L.; Shi, Y.; Ren, L.; Wang, D.; Dai, Y.; Wang, X. Evaluation of Surface Urban Energy and Water Balance Scheme (SUEWS) Using Scaled 2D Model Experiments under Various Seasons and Sky Conditions. *Urban Clim.* **2024**, *54*, 101851. [CrossRef]
2. Piroddu, F.; Lo Cascio, M.; Marras, S.; Sirca, C.; Spano, D. A Systematic Review of Urban Energy Balance Assessments. *Urban Clim.* **2026**, *65*, 102789. [CrossRef]
3. Kim, S.W.; Brown, R.D. Urban Heat Island (UHI) Intensity and Magnitude Estimations: A Systematic Literature Review. *Sci. Total Environ.* **2021**, *779*, 146389. [CrossRef] [PubMed]
4. Cheval, S.; Amihăesei, V.-A.; Chitu, Z.; Dumitrescu, A.; Falcescu, V.; Irașoc, A.; Micu, D.M.; Mihulet, E.; Ontel, I.; Paraschiv, M.-G.; et al. A Systematic Review of Urban Heat Island and Heat Waves Research (1991–2022). *Clim. Risk Manag.* **2024**, *44*, 100603. [CrossRef]
5. Piracha, A.; Chaudhary, M.T. Urban Air Pollution, Urban Heat Island and Human Health: A Review of the Literature. *Sustainability* **2022**, *14*, 9234. [CrossRef]
6. Heaviside, C.; Vardoulakis, S.; Cai, X.M. Attribution of Mortality to the Urban Heat Island during Heatwaves in the West Midlands, UK. *Environ. Health* **2016**, *15*, S27. [CrossRef] [PubMed]
7. Bao, Y.; Li, Y.; Gu, J.; Shen, C.; Zhang, Y.; Deng, X.; Han, L.; Ran, J. Urban Heat Island Impacts on Mental Health in Middle–Aged and Older Adults. *Environ. Int.* **2025**, *199*, 109470. [CrossRef] [PubMed]
8. Wang, S.; Zhan, W.; Zhou, B.; Tong, S.; Chakraborty, T.C.; Wang, Z.; Huang, K.; Du, H.; Middel, A.; Li, J.; et al. Dual Impact of Global Urban Overheating on Mortality. *Nat. Clim. Change* **2025**, *15*, 497–504. [CrossRef]
9. He, J.; Madaniyazi, L.; Chua, P.L.C.; Kim, Y.; Milojevic, A.; Oka, K.; Honda, Y.; Hashizume, M. Impact of the Urban Heat Island on Heat–Related Mortality in the Tokyo Metropolitan Area, Japan. *Environ. Res. Health* **2025**, *3*, 015003. [CrossRef]
10. Huang, Y.; Mao, F.; Xu, Y.; Qi, J.; Zhang, W.; Li, C.; Zhou, M. Association between Urban Heat Islands and Heat–Related Mortality in 70 Pairs of Adjacent Urban–Rural Counties among 8 Topographic Regions in China. *Sustain. Cities Soc.* **2025**, *121*, 106182. [CrossRef]
11. Yuan, Y.; Li, X.; Wang, H.; Geng, X.; Gu, J.; Fan, Z.; Wang, X.; Liao, C. Unraveling the Global Economic and Mortality Effects of Rising Urban Heat Island Intensity. *Sustain. Cities Soc.* **2024**, *116*, 105902. [CrossRef]
12. Srivastava, V.T.; Sharma, A.; Jadon, S.S. A Review of the Formation, Mitigation Strategies from 50 Years of Global Urban Heat Island Studies. *Environ. Dev. Sustain.* **2024**, *28*, 97–114. [CrossRef]
13. Guo, F.; Sun, J.; Hu, D. Surface Energy Balance–Based Surface Urban Heat Island Decomposition at High Resolution. *Remote Sens. Environ.* **2024**, *315*, 114447. [CrossRef]
14. Skelhorn, C.P.; Levermore, G.; Lindley, S.J. Impacts on Cooling Energy Consumption Due to the UHI and Vegetation Changes in Manchester, UK. *Energy Build.* **2016**, *122*, 150–159. [CrossRef]
15. Sussman, H.S.; Dai, A.; Zhou, L. Quantifying the Role of Vegetation on Urban Heat over Bengaluru, India. *Theor. Appl. Climatol.* **2025**, *156*, 104. [CrossRef]
16. Toy, S.; Eren, Z. Spatial Analysis of Sensitive Urban Zones to UHI Formation Through the Parametrization of Urban Features. *Pure Appl. Geophys.* **2025**, *182*, 3831–3856. [CrossRef]
17. Ahmad, B.; Najar, M.B.; Ahmad, S. Analysis of LST, NDVI, and UHI Patterns for Urban Climate Using Landsat–9 Satellite Data in Delhi. *J. Atmos. Sol.-Terr. Phys.* **2024**, *265*, 106359. [CrossRef]
18. Ghosh, S.; Kumar, D.; Kumari, R. Assessing Spatiotemporal Dynamics of Land Surface Temperature and Satellite–Derived Indices for New Town Development and Suburbanization Planning. *Urban Gov.* **2022**, *2*, 144–156. [CrossRef]
19. Wang, C.; Myint, S.W.; Wang, Z.; Song, J. Spatio–Temporal Modeling of the Urban Heat Island in the Phoenix Metropolitan Area: Land Use Change Implications. *Remote Sens.* **2016**, *8*, 185. [CrossRef]

20. Rawal, D.; Gupta, V. Uhi Spatio–Temporal Analysis with Geospatial Techniques: A Case of Ahmedabad City. *Paripex Indian J. Res.* **2021**, *10*, 194–200. [CrossRef]
21. Rao, P.; Singh, A.; Pandey, K. Time–Series Analysis of Open Data for Studying Urban Heat Island Phenomenon: A Geospatial Approach. *Spat. Inf. Res.* **2021**, *29*, 907–918. [CrossRef]
22. Voogt, J.A.; Oke, T.R. Thermal Remote Sensing of Urban Climates. *Remote Sens. Environ.* **2003**, *86*, 370–384. [CrossRef]
23. Mann, H.B. Nonparametric tests against trend. *Econometrica* **1945**, *13*, 245–259. [CrossRef]
24. Kendall, M.G. *Rank Correlation Methods*, 4th ed.; Charles Griffin: San Francisco, CA, USA, 1975.
25. Theil, H.I. A rank–Invariant Method of Linear and Polynomial Regression Analysis. *Indag. Math.* **1950**, *12*, 173.
26. Sen, P.K. Estimates of the Regression Coefficient Based on Kendall's Tau. *J. Am. Stat. Assoc.* **1968**, *63*, 1379–1389. [CrossRef]
27. Gocic, M.; Trajkovic, S. Analysis of changes in meteorological variables using Mann–Kendall and Sen's slope estimator statistical tests. *Glob. Planet. Change* **2013**, *100*, 172–182. [CrossRef]
28. Tan Kesgin, R.İ. Revisiting Trend Stability Using Mann–Kendall and Wilcoxon Signed–Rank Tests Through Innovative Method Comparisons. *Sustainability* **2025**, *17*, 10454. [CrossRef]
29. Fu, P.; Weng, Q. A Time Series Analysis of Urbanization Induced Land Use and Land Cover Change and Its Impact on Land Surface Temperature with Landsat Imagery. *Remote Sens. Environ.* **2016**, *175*, 205–2014. [CrossRef]
30. Tabassum, A.; Kamal, A.S.M.M.; Rahman, M.Z.; Shahid, S. Impact of Urban Sprawl on Urban Heat Island in Chittagong: A Non–Parametric Analysis Using Satellite Nighttime Light and Land Surface Temperature Data for the Period 2000–2021. *Theor. Appl. Climatol.* **2025**, *156*, 341. [CrossRef]
31. Holec, J.; Feranec, J.; Šťastný, P.; Szatmári, D.; Kopecká, M.; Garaj, M. Evolution and Assessment of Urban Heat Island between the Years 1998 and 2016: Case Study of the Cities Bratislava and Trnava in Western Slovakia. *Theor. Appl. Climatol.* **2020**, *141*, 979–997. [CrossRef]
32. Kopecká, M.; Szatmári, D.; Holec, J.; Feranec, J. Urban Heat Island Modelling Based on MUKLIMO: Examples from Slovakia. *Agil. GIScience Ser.* **2021**, *2*, 5. [CrossRef]
33. Uhrin, A.; Onačillová, K. Spatiotemporal analysis of land surface temperature and land cover changes in Prešov city using downscaling approach and machine learning algorithms. *Environ. Monit. Assess.* **2025**, *197*, 126. [CrossRef] [PubMed]
34. Onačillová, K.; Gallay, M. Spatio–temporal analysis of surface urban heat island based on Landsat ETM+ and OLI/TIRS imagery in the city of Košice, Slovakia. *Carpathian J. Earth Environ. Sci.* **2018**, *13*, 395–408. [CrossRef]
35. Hofierka, J.; Gallay, M.; Onačillová, K.; Hofierka, J., Jr. Physically–based land surface temperature modeling in urban areas using a 3-D city model and multispectral satellite data. *Urban Clim.* **2020**, *31*, 100566. [CrossRef]
36. Onačillová, K.; Fedor, T.; Gallay, M.; Šašak, J.; Bogľarský, J.; Kaňuk, J.; Salajová, N. Local climate zones and diurnal surface heating in a Central European city: A comparison of Landsat, ECOSTRESS, and ENVI–met with in situ measurements in Košice (Slovakia). *Remote Sens. Appl. Soc. Environ.* **2026**, *41*, 101933. [CrossRef]
37. Fedor, T.; Hofierka, J. Estimating Heat Stress in the Urban Centre of Košice Using ENVI–Met and High–Resolution Surface Data. *Geogr. Cassoviensis* **2025**, *19*, 81–94. [CrossRef]
38. Svetozarov, N.; Gallay, M. Porovnanie 2D a 3D Prístupu Pri Hodnotení Množstva Stromovej Zelene v Meste Košice Pomocou Dát z Leteckého Laserového Skenovania. *Geogr. J.* **2024**, *76*, 221–247. [CrossRef]
39. Priatková, A.; Sekan, J.; Tamáska, D.M. The Urban Planning of Košice and the Development of a 20th Century Avenue. *Archit. Urban.* **2020**, *54*, 70–88. [CrossRef]
40. Sýkora, L. Proměny postsocialistických metropolí. *Geogr. Rozhl.* **2014**, *23*, 2–5.
41. Mesto Košice. Územný Plán Mesta Košice. Available online: https://opendata.kosice.sk/pages/uzemny-plan (accessed on 23 April 2026).
42. SHMI (Slovak Hydrometeorologic Institute). *Climate Atlas of Slovakia*; Slovak Hydrometeorological Institute: Bratislava, Slovakia, 2015; p. 228.
43. Copernicus Land Monitoring Service. Available online: https://land.copernicus.eu/en/products/corine–land–cover (accessed on 2 February 2026).
44. Yue, S.; Hashino, M. Long Term Trends of Annual and Monthly Precipitation in Japan. *J. Am. Water Resour. Assoc.* **2003**, *39*, 587–596. [CrossRef]
45. Singh, P.; Kumar, V.; Thomas, T.; Arora, M. Basin–Wide Assessment of Temperature Trends in Northwest and Central India. *Hydrol. Sci. J.* **2008**, *53*, 421–433. [CrossRef]
46. Yue, S.; Wang, C.Y. The Mann–Kendall Test Modified by Effective Sample Size to Detect Trend in Serially Correlated Hydrological Series. *Water Resour. Manag.* **2004**, *18*, 201–2018. [CrossRef]
47. Rani, M.; Kumar, P.; Pandey, P.C.; Srivastava, P.K.; Chaudhary, B.S.; Tomar, V.; Mandal, V.P. Multi–Temporal NDVI and Surface Temperature Analysis for Urban Heat Island Inbuilt Surrounding of Sub–Humid Region: A Case Study of Two Geographical Regions. *Remote Sens. Appl. Soc. Environ.* **2018**, *10*, 163–172. [CrossRef]

48. Cetin, M.; Ozenen Kavlak, M.; Senyel Kurkcuoglu, M.A.; Bilge Ozturk, G.; Cabuk, S.N.; Cabuk, A. Determination of Land Surface Temperature and Urban Heat Island Effects with Remote Sensing Capabilities: The Case of Kayseri, Türkiye. *Nat. Hazards* **2024**, *120*, 5509–5536. [CrossRef]
49. Chen, X.L.; Zhao, H.M.; Li, P.X.; Yin, Z.Y. Remote Sensing Image–Based Analysis of the Relationship between Urban Heat Island and Land Use/Cover Changes. *Remote Sens. Environ.* **2006**, *104*, 133–146. [CrossRef]
50. Zha, Y.; Gao, J.; Ni, S. Use of normalized difference built–up index in automatically mapping urban areas from TM imagery. *Int. J. Remote Sens.* **2003**, *24*, 583–594. [CrossRef]
51. Roose, A.; Kull, A.; Gauk, M.; Tali, T. Land Use Policy Shocks in the Post–Communist Urban Fringe: A Case Study of Estonia. *Land Use Policy* **2013**, *30*, 76–83. [CrossRef]
52. Stanilov, K. The restructuring of non–residential uses in the post–socialist metropolis. In *The Post–Socialist City: Urban Form and Space Transformations in Central and Eastern Europe after Socialism; GeoJournal Library*; Stanilov, K., Ed.; Springer: Dordrecht, The Netherlands, 2007; Volume 92, pp. 73–99. [CrossRef]
53. Sandu, A. The Post–Socialist Cities from Central and Eastern Europe: Between Spatial Growth and Demographic Decline. *Urban Stud.* **2024**, *61*, 821–837. [CrossRef]
54. Sieber, A.; Kuemmerle, T.; Prishchepov, A.V.; Wendland, K.J.; Baumann, M.; Radeloff, V.C.; Baskin, L.M.; Hostert, P. Landsat–Based Mapping of Post–Soviet Land–Use Change to Assess the Effectiveness of the Oksky and Mordovsky Protected Areas in European Russia. *Remote Sens. Environ.* **2013**, *133*, 38–51. [CrossRef]
55. Badraghi, A.; Krůček, M.; Král, K.; Reitschmiedová, E.; Šálek, V.; Kotápišová, M.; Novotná, B.; Frouz, J. Woody Species Succession and Spontaneous Forest Development in Post–Mining Sites after Coal Mining in the Czech Republic. *Ecol. Eng.* **2023**, *194*, 107051. [CrossRef]
56. Černý, J.; Daňková, T.; Mudrák, O.; Spurná, V.; Frouz, J. Establishment, Survival, and Growth of Beech, Oak, and Spruce Seedlings During Unassisted Forest Recovery in Post–Mining Sites. *Forests* **2025**, *16*, 1651. [CrossRef]
57. Chaddad, F.; Mello, F.A.O.; Tayebi, M.; Safanelli, J.L.; Campos, L.R.; Amorim, M.T.A.; Sousa, G.P.B.; Ferreira, T.O.; Ruiz, F.; Perlatti, F.; et al. Impact of Mining–Induced Deforestation on Soil Surface Temperature and Carbon Stocks: A Case Study Using Remote Sensing in the Amazon Rainforest. *J. S. Am. Earth Sci.* **2022**, *119*, 103983. [CrossRef]
58. Bujalský, L.; Jirka, V.; Zemek, F.; Frouz, J. Relationships between the Normalised Difference Vegetation Index and Temperature Fluctuations in Post–Mining Sites. *Int. J. Min. Reclam. Environ.* **2018**, *32*, 254–263. [CrossRef]
59. Erthalia, M.; Supriatna; Damayanti, A. Remote Sensing and GIS for Land Conservation: Identification of Post–Tin Mining Land Conservation in Perimping Sub Watershed. *IOP Conf. Ser. Earth Environ. Sci.* **2019**, *311*, 012019. [CrossRef]
60. Alibakhshi, S.; Cook–Patton, S.C.; Davin, E.; Maeda, E.E.; Araújo, M.B.; Heinlein, D.; Heiskanen, J.; Pellikka, P.; Crowther, T.W. Natural Forest Regeneration Is Projected to Reduce Local Temperatures. *Commun. Earth Environ.* **2024**, *5*, 577. [CrossRef]
61. Guha, S.; Govil, H.; Dey, A.; Gill, N. Analytical Study of Land Surface Temperature with NDVI and NDBI Using Landsat 8 OLI and TIRS Data in Florence and Naples City, Italy. *Eur. J. Remote Sens.* **2018**, *51*, 667–678. [CrossRef]
62. Tiwari, A.K.; Kanchan, R. Analytical Study on the Relationship among Land Surface Temperature, Land Use/Land Cover and Spectral Indices Using Geospatial Techniques. *Discov. Environ.* **2024**, *12*, 101269. [CrossRef]
63. Kumar, D.; Shekhar, S. Statistical Analysis of Land Surface Temperature–Vegetation Indexes Relationship through Thermal Remote Sensing. *Ecotoxicol. Environ. Saf.* **2015**, *121*, 39–44. [CrossRef] [PubMed]
64. Malik, M.S.; Shukla, J.P.; Mishra, S. Relationship of LST, NDBI and NDVI Using Landsat–8 Data in Kandaihimmat Watershed, Hoshangabad, India. *Indian J. Geo-Mar. Sci.* **2019**, *48*, 25–31.
65. As–syakur, A.R.; Adnyana, I.W.S.; Arthana, I.W.; Nuarsa, I.W. Enhanced Built–UP and Bareness Index (EBBI) for Mapping Built–UP and Bare Land in an Urban Area. *Remote Sens.* **2012**, *4*, 2957–2970. [CrossRef]
66. Liu, Y.; Meng, Q.; Zhang, L.; Wu, C. NDBSI: A Normalized Difference Bare Soil Index for Remote Sensing to Improve Bare Soil Mapping Accuracy in Urban and Rural Areas. *Catena* **2022**, *214*, 106265. [CrossRef]
67. Yuan, F.; Bauer, M.E. Comparison of Impervious Surface Area and Normalized Difference Vegetation Index as Indicators of Surface Urban Heat Island Effects in Landsat Imagery. *Remote Sens. Environ.* **2007**, *106*, 375–386. [CrossRef]
68. Huang, C.; Ye, X. Spatial Modeling of Urban Vegetation and Land Surface Temperature: A Case Study of Beijing. *Sustainability* **2015**, *7*, 9478–9504. [CrossRef]
69. Ferreira, L.S.; Duarte, D.H.S. Exploring the Relationship between Urban Form, Land Surface Temperature and Vegetation Indices in a Subtropical Megacity. *Urban Clim.* **2019**, *27*, 105–123. [CrossRef]
70. Stumpe, B.; Bechtel, B.; Heil, J.; Jörges, C.; Jostmeier, A.; Kalks, F.; Schwarz, K.; Marschner, B. Soil Texture Mediates the Surface Cooling Effect of Urban and Peri–Urban Green Spaces during a Drought Period in the City Area of Hamburg (Germany). *Sci. Total Environ.* **2023**, *897*, 165228. [CrossRef] [PubMed]
71. Soltanifard, H.; Amani-Beni, M. The Cooling Effect of Urban Green Spaces as Nature–Based Solutions for Mitigating Urban Heat: Insights from a Decade–Long Systematic Review. *Clim. Risk Manag.* **2025**, *49*, 100731. [CrossRef]

72. Ma, W.; Yu, Z.; Chen, J.; Yang, W.; Zhang, Y.; Hu, Y.; Shao, M.; Hu, J.; Zhang, Y.; Zhang, H.; et al. What Drives the Cooling Dynamics of Urban Vegetation via Evapotranspiration and Shading under Extreme Heat? *Sustain. Cities Soc.* **2025**, *130*, 106659. [CrossRef]
73. Alonzo, M.; Ibsen, P.C.; Locke, D.H. Urban Trees and Cooling: A Review of the Recent Literature (2018 to 2024). *Arboric. Urban For.* **2025**, *51*, 420–444. [CrossRef]

Disclaimer/Publisher's Note: The statements, opinions and data contained in all publications are solely those of the individual author(s) and contributor(s) and not of MDPI and/or the editor(s). MDPI and/or the editor(s) disclaim responsibility for any injury to people or property resulting from any ideas, methods, instructions or products referred to in the content.